Redox Characterization of *Geobacter sulfurreducens* Cytochrome c_7: Physiological Relevance of the Conserved Residue F15 Probed by Site-Specific Mutagenesis†

Miguel Pessanha,‡ Yuri Y. Londer,§ W. Chris Long,§ Jill Erickson,§ P. Raj Pokkuluri,§ Marianne Schiffer,§ and Carlos A. Salgueiro*,‡,||

Instituto de Tecnologia Química e Biológica, Universidade Nova de Lisboa, Rua da Quinta Grande 6, 2780-156 Oeiras, Portugal, Biosciences Division, Argonne National Laboratory, Argonne, Illinois 60439, and Departamento de Química da Faculdade de Ciências e Tecnologia da Universidade Nova de Lisboa, Quinta da Torre, 2829-516, Portugal

Received April 9, 2004; Revised Manuscript Received June 4, 2004

ABSTRACT: The complete genome sequence of the δ-proteobacterium *Geobacter sulfurreducens* reveals a large abundance of multiheme cytochromes. Cytochrome c_7, isolated from this metal ion-reducing bacterium, is a triheme periplasmic electron-transfer protein with M_r 9.6 kDa. This protein is involved in metal ion-reducing pathways and shares 56% sequence identity with a triheme cytochrome isolated from the closely related δ-proteobacterium *Desulfuromonas acetoxidans* (Dac_7). In this work, two-dimensional NMR was used to monitor the heme core and the general folding in solution of the *G. sulfurreducens* triheme cytochrome c_7 (PpcA). NMR signals obtained for the three hemes of PpcA at different stages of oxidation were cross-assigned to the crystal structure [Pokkuluri, P. R., Londer, Y. Y., Duke, N. E. C., Long, W. C., and Schiffer, M. (2004) *Biochemistry 43*, 849−859] using the complete network of chemical exchange connectivities, and the order in which each heme becomes oxidized was determined at pH 6.0 and 8.2. Redox titrations followed by visible spectroscopy were also performed in order to monitor the macroscopic redox behavior of PpcA. The results obtained showed that PpcA and Dac_7 have different redox properties: (i) the order in which each heme becomes oxidized is different; (ii) the reduction potentials of the heme groups and the global redox behavior of PpcA are pH dependent (redox−Bohr effect) in the physiological pH range, which is not observed with Dac_7. The differences observed in the redox behavior of PpcA and Dac_7 may account for the different functions of these proteins and constitute an excellent example of how homologous proteins can perform different physiological functions. The redox titrations followed by visible spectroscopy of PpcA and two mutants of the conserved residue F15 (PpcAF15Y and PpcAF15W) lead to the conclusion that F15 modulates the redox behavior of PpcA, thus having an important physiological role.

The microorganisms belonging to the *Geobacteraceae* family play important roles in several metal biogeochemical cycles and also in the bioremediation of radioactive metals (*1*). Indeed, the members of this bacterial family can degrade natural and contaminant organic matter coupled to the reduction of a large variety of alternative terminal electron acceptors, including metal oxides of Cr(VI), U(VI), and Fe(III). This feature presents opportunities for the development of new bioremediation strategies for removing toxic chemicals from subsurface environments, by directly reducing soluble toxic metal oxides such as Cr(VI) and radioactive soluble contaminants such as U(VI) to insoluble oxides [(Cr(III) and U(IV)], facilitating the removal of metal pollutants from the environment. Another peculiarity of these microorganisms is their ability to reduce and dissolve insoluble metal oxides (Fe(III)) coupled to the oxidation of organic carbon (*2*−*6*).

The genome sequence of the bacterium *Geobacter sulfurreducens* was recently completed and reveals that the bacterium encodes for large numbers of multiheme *c*-type cytochromes (*1*). The abundance of multiheme cytochromes, most of them located in the periplasm or in the outer membrane, suggests that the electron transport pathways in those bacteria are extremely versatile, allowing a precise and adequate physiological response to the diverse metal ions they can find in the natural environments.

To understand those electron transfer pathways, it is first necessary to characterize the individual components of the electron-transfer chain, which are mainly composed of heme proteins. Various cytochromes isolated from *Geobacter* bacterium are involved in metal reduction, but little is known about the electron-transfer mechanisms (*8*−*13*). One of those

† This work is supported by FCT-Portugal Grant POCTI/42902/QUI/2001 (approved by FCT and POCTI and cofinanced by FEDER) and by the U.S. Department of Energy's Office of Science, Biological and Environmental Research, Structural Biology and NABIR programs, under Contract W-31-109-Eng-38. Miguel Pessanha acknowledges Fundação para a Ciência e Tecnologia (FCT), Portugal, for a doctoral fellowship (SFRH/5229/2001).

* To whom correspondence should be addressed. Telephone: (351) 214 469 848. Fax: (351) 214 428 766. E-mail: cas@itqb.unl.pt.

‡ Instituto de Tecnologia Química e Biológica, Universidade Nova de Lisboa.

§ Argonne National Laboratory.

|| Departamento de Química da Faculdade de Ciências e Tecnologia da Universidade Nova de Lisboa.

10.1021/bi0492859 CCC: $27.50
Published on Web 07/09/2004

is the periplasmatic triheme cytochrome, cytochrome c_7, which was purified from *G. sulfurreducens* and *Geobacter metallireducens* bacteria (*13*, *14*). The *G. sulfurreducens* triheme cytochrome c_7 (PpcA)[1] is involved in the reduction of metal ion species such as Fe(III) and U(VI) (*11*). The gene that encodes for this cytochrome was cloned and overexpressed in *Escherichia coli* (*15*). PpcA is a small protein with 71 residues containing three *c*-type hemes with bis-histidinyl axial coordination, and its crystal structure was recently determined (*16*).

A homologue triheme cytochrome c_7, isolated from the periplasm of the sulfur-reducing bacterium *Desulfuromonas acetoxidans*, Dac_7, has been the subject of several biochemical studies (*17*−*19*). Although a sulfur reductase activity has been associated with this cytochrome (*20*), the physiological function of Dac_7 is still debated, and it was proposed (*21*) that it might be similar to that of tetraheme cytochrome c_3 in sulfate-reducing bacteria, which is the partner of the periplasmic hydrogenase. The crystal structure of Dac_7 (*22*) shows that the arrangement of the three hemes is conserved, when compared with the heme core of tetraheme cytochromes c_3 isolated from the *Desulfovibrionacea* family (for a revision see ref *23*), with heme II deleted. Thus, in order not to confuse the literature, throughout this article the PpcA heme groups are numbered I, III, and IV, by analogy to the structurally homologous hemes in tetraheme cytochromes c_3.

The comparison of PpcA and Dac_7 crystal structures shows that the spatial disposition of hemes III and IV is conserved, but the relative location of heme I is quite different (*16*). Hemes I and III and the conserved phenylalanine residue F15 situated nearby form a structural motif that is present not only in PpcA and Dac_7 but also in the other four homologues of PpcA (*16*) and in cytochrome c_7 polymeric forms, both isolated from *G. sulfurreducens* (*24*), and in tetraheme cytochromes c_3.

In this work, the heme core and the general folding of PpcA in solution were monitored by NMR, and the order of oxidation of the three hemes was fully cross-assigned to the crystal structure, for the first time in a multiheme cytochrome isolated from *Geobacter* spp. Furthermore, the influence of the conserved residue F15 on the redox behavior of this protein was monitored by studying two F15 mutants of PpcA.

MATERIALS AND METHODS

Sample Preparations. *G. sulfurreducens* cytochrome c_7 was produced in *E. coli* and purified by cation exchange and gel filtration as described previously (*15*, *16*). To prepare the F15 mutants (PpcAF15Y and PpcAF15W), the QuikChange site-directed mutagenesis kit (Stratagene) was used. Purification of the mutants was performed following the same procedure used for the wild-type strain.

For NMR experiments carried out on the fully reduced and fully oxidized PpcA, the protein solution buffer was exchanged to 99.9% ^2H_2O using ultrafiltration methods (Amicon; YM-10); the final concentration is approximately 1 mM. For NMR experiments of partially oxidized sample, the experimental conditions of the sample were optimized (lowering protein concentration down to 0.5 mM, increasing ionic strength up to 500 mM, and lowering temperature down to 274 K) to allow the observation of the heme NMR signals in all oxidation stages.

The reduced sample was obtained by adding gaseous hydrogen in the presence of catalytic amounts of Fe-hydrogenase isolated from *Desulfovibrio vulgaris* (Hildenborough). The partially oxidized samples, used for NMR redox titrations, were obtained by first removing the hydrogen from the reduced sample with argon and then adding controlled amounts of air into the NMR tube with a syringe through the serum caps.

For the reduced and partially oxidized samples, the pH was adjusted inside an anaerobic chamber (Mbraun MB 150 I) by addition of small amounts of NaO^2H or ^2HCl. The pH values reported are direct meter readings without correction for the isotope effect.

NMR Studies of PpcA and Its F15 Mutants. ^1H NMR spectra were obtained on a Bruker DRX500 spectrometer equipped with a 5 mm inverse detection probe head with internal B_0 gradient coils and a Eurotherm 818 temperature control unit. Two-dimensional spectra of PpcA were acquired at different temperatures (274 and 285 K) at pH 6.0 and 8.2. All the 2D-NMR spectra were acquired collecting 4096 (t_2) × 512 (t_1) data points to cover a sweep width of 7 kHz, with 128 scans per increment. The ^2H_2O nuclear Overhauser enhancement spectroscopy (NOESY) spectra with 50 and 100 ms mixing time, total correlation spectroscopy (TOCSY) spectra with 40 and 60 ms mixing time, and correlation spectroscopy (COSY) spectra were acquired using standard pulse techniques. ^1H chemical shifts were calibrated using the water signal as internal reference.

NOESY and TOCSY spectra were carried out on the fully reduced mutated proteins PpcAF15W and PpcAF15Y using identical acquisition and processing parameters to those of wild-type cytochrome.

Redox Titrations of PpcA Followed by NMR. The pattern of reoxidation for each heme methyl group at 274 K at both pH 6.0 and 8.2 was observed in 2D-exchange spectroscopy (EXSY) experiments performed with 25 ms mixing time, using 4096 (t_2) × 512 (t_1) data points to cover a sweep width of 22.5 kHz, with 128 scans per increment.

Redox Titrations Followed by Visible Spectroscopy. Anaerobic redox titrations of PpcA, PpcAF15W, and PpcAF15Y were performed as described previously (*25*) with ∼18 μM protein solutions in 100 mM TRIS/maleate buffer at pH 6.9 and 7.9. To check for hysteresis, each redox titration was performed in both oxidative and reductive directions. To ensure a good equilibrium between the redox centers and the working electrode (*26*), a mixture of the following redox mediators was added to the protein solution, all at ∼4 μM final concentration: methylene blue, gallocyanine, indigo tetrasulfonate, indigo trisulfonate, indigo disulfonate, anthraquinone-2,7-disulfonate, 2-hydroxy-1,4-naphthoquinone, anthraquinone-2-sulfonate, safranine O, diquat, benzyl viologen, neutral red, and methyl viologen. The solution potentials were measured using a combined Pt/Ag/AgCl electrode, calibrated with the quinhydrone couple, and the visible spectra were recorded at 298 ± 1 K in a Shimadzu UV-1203 spectrophotometer, placed inside an anaerobic glovebox with O_2 levels kept at <0.5 ppm. The reduced fraction of the PpcA and mutated cytochromes was deter-

[1] Abbreviations: PpcA, *Geobacter sulfurreducens* triheme cytochrome c_7; Dac_7, *Desulfuromonas acetoxidans* triheme cytochrome; NOESY, nuclear Overhauser enhancement spectroscopy; TOCSY, total correlation spectroscopy; COSY, correlation spectroscopy.

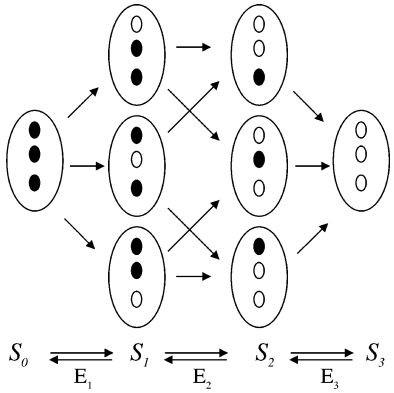

FIGURE 1: Model for the electronic distribution in a triheme protein. The inner circles represent the three heme groups that can be reduced (black circles) or oxidized (open circles). E_1, E_2, and E_3 are the macroscopic reduction potentials connecting the four stages of oxidation (S_{0-3}), each including the microstates with the same number of oxidized hemes.

mined using the α band peak at 551 nm. The optical contribution of the mediators was subtracted by measuring the height of the peak at 551 nm relative to the straight line connecting the two isosbestic points (541 and 559 nm) flanking the α band according to the method described in the literature (*25*).

For each protein, the experiments were performed at least two times, and the reduction potentials were found to be reproducible within ±2 mV.

Model for Calculation of the Macroscopic Reduction Potentials. In the particular case of a triheme cytochrome, three consecutive reversible steps of one-electron transfer convert the fully reduced state (stage 0) to the fully oxidized state (stage 3). Therefore, four macroscopic redox stages are defined, and the relative populations of the four stages at equilibrium, for any solution potential, are defined by three macroscopic reduction potentials (E_1, E_2, and E_3) according to the Nernst equation (Figure 1). The three macroscopic reduction potentials can be obtained by fitting the experimental variation of the total reduced fraction of the protein at each solution potential. This theoretical model has been successfully applied to the determination of macroscopic reduction potentials of several multiheme cytochromes (*27*−*30*).

In previous studies (*31*), it was possible to further extend the model to the calculation of the absolute values for microscopic redox potential, heme−heme redox interactions, and redox−Bohr interactions by fitting the pH dependence of the observed heme methyl group paramagnetic shifts and visible data sets (*32*). However, in the particular case of PpcA, only at very low temperature values it was possible to obtain the NMR data to monitor the heme redox behavior in all redox stages. Unfortunately, under these experimental conditions it was not possible to obtain stable visible redox titrations and, therefore, to obtain data with the necessary quality to be used in the calibration of the relative heme reduction and heme interaction potentials.

RESULTS AND DISCUSSION

Cross Assignment of Individual Heme Resonances to the Three-Dimensional Structure. The specific assignments of the individual heme proton resonances in the reduced form of PpcA (Table 1) were made by examining the interheme

Table 1: Proton Chemical Shifts of Heme Substituents and Aromatic Resonances in *Geobacter sulfurreducens* Triheme Ferrocytochrome, at pH 6.0 and 274 K[a]

	heme I	heme III	heme IV
5H	9.75	10.67	9.10
10H	9.24	9.95	9.41
15H	9.33	9.54	9.49
20H	9.60	10.22	9.50
2^1CH_3	3.64	4.43	3.71
7^1CH_3	3.66	4.22	3.10
12^1CH_3	2.63	3.59	4.04
18^1CH_3	3.44	3.92	3.42
3^1H	6.39	6.98	6.12
8^1H	6.40	6.68	6.35
3^2CH_3	2.19	1.76	2.14
8^2CH_3	1.88	3.07	1.62
aromatic protons			
F15 (2-H)	5.67		
(3-H)	6.33		
(4-H)	6.02		
(5-H)	1.88		
(6-H)	6.30		
F41 (2,6-H)	7.77		
(3,5-H)	8.11		
(4-H)	8.41		

[a] The hemes and aromatic protons are numbered according to IUPAC−IUB nomenclature for tetrapyrroles (*45*).

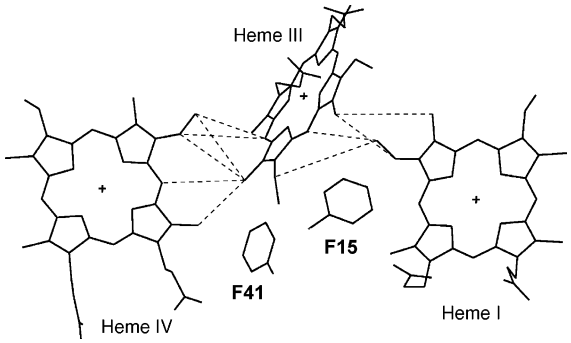

FIGURE 2: Heme core architecture of the *Geobacter sulfurreducens* PpcA. Dashed lines indicate the interheme NOEs used in the specific assignments of the heme protons in the reduced cytochrome. To clarify the text, residues F15 and F41 are also shown.

NOE connectivities in the 50 and 100 ms NOESY spectra obtained for the reduced protein. To validate the assignments, the observed proton interheme connectivities were then compared with the distances obtained from the crystal structure of PpcA (*16*). The observed proton interheme connectivities agree with the ones expected from the crystal structure heme core, and they are illustrated in Figure 2. Two exceptions were found, for protons $8^2CH_3^{III}$ and 8^1H^{III}, which do not show the expected connectivities for $8^2CH_3^{I}$ and $7^1CH_3^{I}$, respectively.

The assignment of the heme protons was also confirmed by the analysis of the NOEs observed between those protons and the aromatic ring protons from residues not coordinated to heme groups. The amino acid sequence of PpcA (*11*) reveals that, besides the His axial heme ligands, only two other aromatic residues are present: F15 and F41. The assignment of each phenylalanine residue was straightforward (Table 1) by comparing the aromatic region in the NOESY reduced spectra of PpcA and PpcAF15Y (cf. Figure 3). The conserved residue F15 is immobilized between hemes I and III, and therefore, its aromatic resonances are broadened and the five aromatic protons distinguishable (Table 1). The

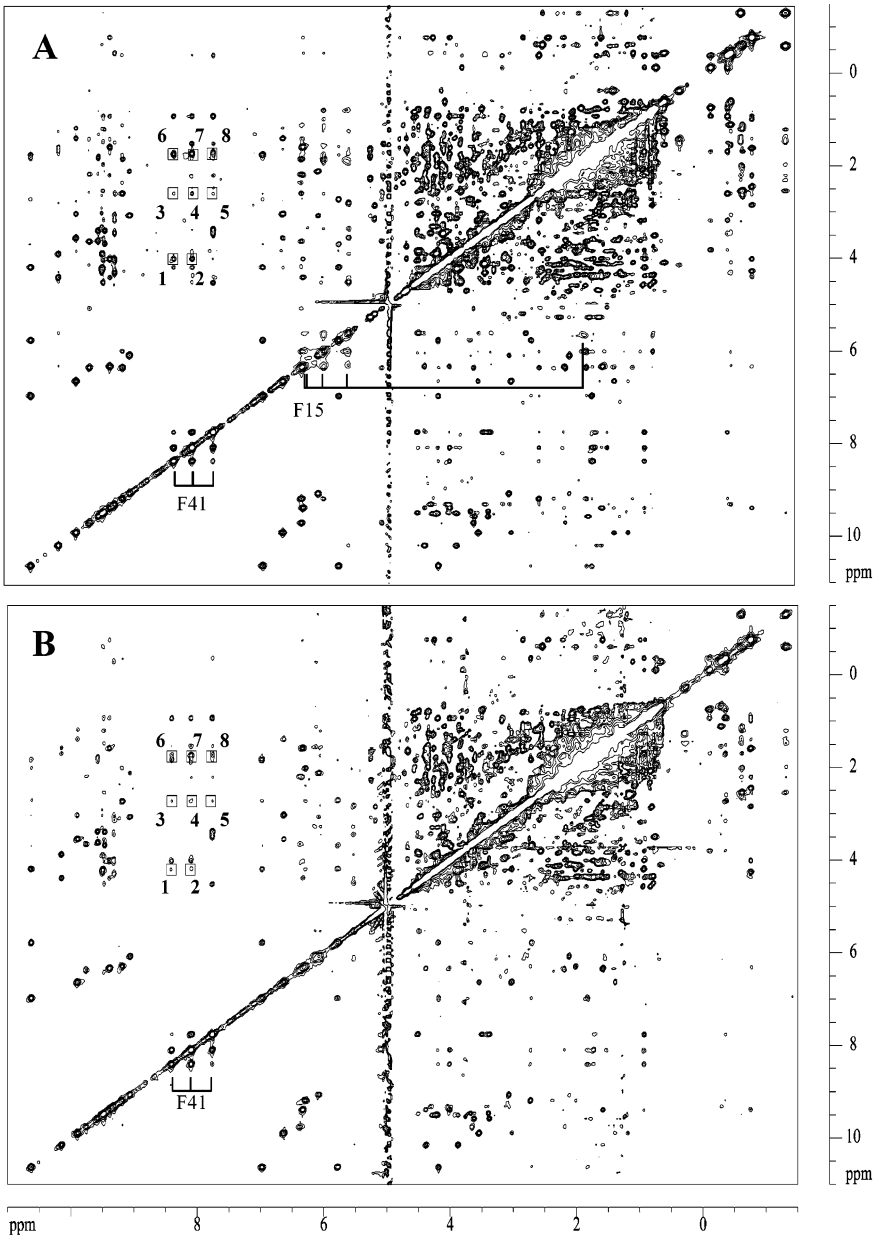

FIGURE 3: Regions of NOESY spectra of PpcA (A) and PpcAF15Y (B) in the reduced form at 274 K and pH 6.0. The aromatic ring protons of F41 and F15 are indicated. Connectivities between the assigned aromatic protons of F41 and heme protons are indicated: 1 and 2 show the connectivities between F41 aromatic protons and $12^1CH_3^{IV}$; 3, 4, and 5 connect F41 aromatic protons and $12^1CH_3^I$; 6, 7, and 8 indicate the connectivities between F41 aromatic protons and $3^2CH_3^{III}$.

unusual low field chemical shifts observed for F15 aromatic protons are due to the large ring current effects produced by hemes I and III.

The observed connectivities between the aromatic protons of both F15 (data not shown) and F41 and those of the heme protons (Figure 3) are in agreement with the crystal structure, confirming the assignment of the individual heme proton resonances. Additional connectivities between F41 aromatic ring protons and the heme methyl group $12^1CH_3^I$ are observed (Figure 3).

The comparison of PpcA and *Dac*$_7$ crystal structures shows that the general fold of both proteins is similar, except for the specific region comprising residues E32−F41. This is not surprising when it is taken into account that those proteins share 56% identity and conserve the relative location of the axial ligands and heme binding motifs (*16*). However, the spatial position of heme I in PpcA and *Dac*$_7$ is different, probably due to the insertion of two extra residues before and after the binding site of heme I (*16*). In fact, the edge-to-edge distance between hemes I and IV is larger in PpcA (13.6 Å) when compared with *Dac*$_7$ (11.4 Å); it increases by approximately 2 Å the distance between the heme methyls $12CH_3^I$ and $12CH_3^{IV}$. This observation is corroborated by the NMR data, since, in contrast to what was observed in *Dac*$_7$ (*18*), no NOE connectivity is observed between heme methyls $12CH_3^I$ and $12CH_3^{IV}$ in PpcA (cf. Figure 2).

The accuracy of the heme proton assignment was tested by comparing the observed heme proton chemical shifts with the calculated ones from the crystal structure of PpcA (Figure 4). These shifts correlate well even for the protons subject to the larger ring current shifts, such as $8^2CH_3^I$, $2^1CH_3^{III}$, and $8^2CH_3^{IV}$, showing that the solution and crystal structures are similar and that the overall heme core architecture and protein folding are essentially maintained in solution.

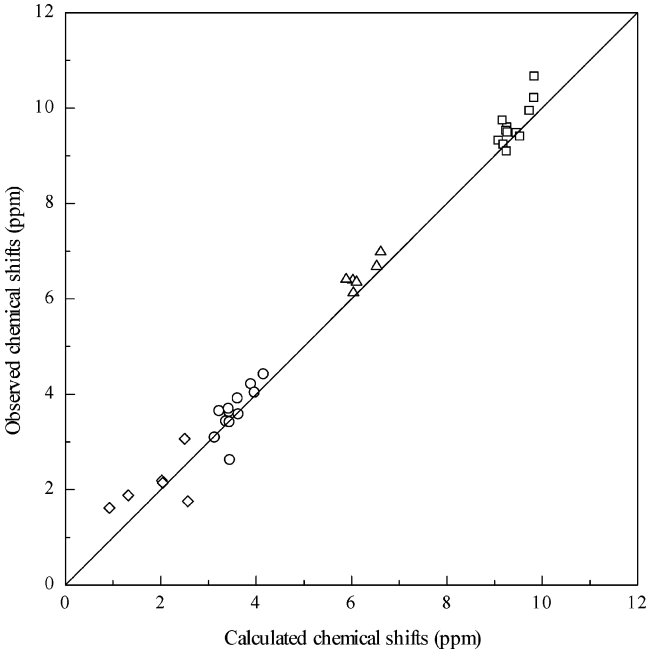

FIGURE 4: Comparison between the calculated and observed chemical shifts for the heme substituents of reduced PpcA. The chemical shifts of the heme substituents were calculated by correcting the heme protons' reference shifts (9.36 ppm for meso protons, 6.13 ppm for thioether methines, 3.48 ppm for methyls, and 2.12 ppm for thioether methyls (*42*)) with the ring current shifts calculated from the PpcA crystal structure (*16*), according to the procedures described by Messias et al. (*43*) and Turner et al. (*44*). The meso protons, thioether methines, methyls, and thioether methyls are represented by squares, triangles, circles, and diamonds, respectively. The dashed line has a unit slope.

Order of Oxidation of the Heme Groups. All the heme irons of PpcA have bis-histidinyl axial coordination and are low spin in both the reduced and oxidized forms. Thus, the protein is diamagnetic when reduced (Fe(II), $S = 0$) and paramagnetic when oxidized (Fe(III), $S = {}^1/_2$). These features are convenient for NMR studies, since widely different well-resolved spectra are obtained for both oxidation states, making it possible to assign the order by which the hemes are oxidized. Nonetheless, the full assignment of the heme order of oxidation depends on the intermolecular electron exchange rate, which should be intermediate to slow, on the NMR time scale, so that signals of different heme groups can be followed throughout the complete reoxidation (*33*). However, PpcA shows both fast intra- and intermolecular electron exchange on the NMR time scale (data not shown) under the typical experimental conditions used for related studies in several multiheme cytochromes (protein concentration in the range 1−2 mM, 298 K, and 100 mM ionic strength), and thus, it was not possible to obtain NMR cross-peaks for the heme groups in all oxidation stages due to excessive exchange broadening of the NMR signals. To overcome this difficulty, the experimental conditions of the sample were optimized (decreasing protein concentration, increasing ionic strength, and decreasing temperature) and monitored by EXSY NMR. This optimization study showed that the experimental conditions which allow the observation of the heme NMR signals in all oxidation stages for PpcA are (i) ionic strength 500 mM NaCl, (ii) protein concentration 0.5 mM, and (iii) temperature 274 K. Under these optimized experimental conditions, the minimum and maximum values for the intra- and intermolecular electronic exchange are 3.8×10^4 s^{-1} and 4.7×10^3 s^{-1}, respectively, allowing the averaging of the signals of the eight redox microstates in four groups of macroscopic oxidation stages (Figure 1). The substituents of each heme have different chemical shifts in the four macroscopic oxidation stages, and since these paramagnetic shifts are proportional to the degree of oxidation of that particular heme group, they can be used to monitor the oxidation of each heme throughout a redox titration (*33*, *34*).

Table 2: Redox-Dependent Heme Methyl Chemical Shifts in the Triheme Cytochrome from *G. sulfurreducens*, at pH 6.0 and 8.2 (Values Indicated in Parentheses)[a]

oxidation stage	chemical shift (ppm)			x_i			
	I	III	IV	I	III	IV	Σx_i
0	2.63	4.22	4.04	0	0	0	0
	(2.63)	(4.22)	(4.04)	(0)	(0)	(0)	
1	14.76	7.32	n.o.	0.600	0.208	0.192[c]	1
	(11.12)	(n.o.)[b]	(10.97)	(0.426)	(0.153)[c]	(0.421)	(1)
2	21.38	10.76	12.18	0.927	0.438	0.573	1.94
	(20.49)	(7.84)	(17.53)	(0.897)	(0.241)	(0.819)	(1.96)
3	22.85	19.14	18.25	1	1	1	3
	(22.55)	(19.22)	(20.52)	(1)	(1)	(1)	(3)

[a] The heme methyls $12^1CH_3^I$, $7^1CH_3^{III}$, and $12^1CH_3^{IV}$ were chosen to monitor each heme oxidation through the four oxidation stages. The heme fractions of oxidation, x_i, in each stage of oxidation are calculated accordingly to the equation $x_i = (\delta_i - \delta_0)/(\delta_3 - \delta_0)$, where δ_i, δ_0, and δ_3 are the observed chemical shifts of the heme methyl in stages i, 0, and 3, respectively (*33*). [b] n.o. = not observed. [c] Estimated values (see text).

As the reoxidation of a multihem protein proceeds, the heme methyl signals become very shifted from the diamagnetic region of the spectra, thus being the most adequate heme substituents to monitor a reoxidation by exchange NMR spectroscopy (*33*). In the case of PpcA, the heme I signals in oxidation stage 1 are sharp enough to allow the observation of strong cross-peaks connecting the methyl signals of heme I in stages 0 and 1. On the contrary, for hemes III and IV, the existence of broader signals in oxidation stage 1 does not allow the observation of exchange cross-peaks between stages 0 and 1, preventing the assignment of the signals to stage 0. However, in the fully oxidized stage (stage 3) the heme methyl signals are again sharp enough to give exchange NMR cross-peaks connecting stages 3, 2, and 1. Thus, to make it possible to monitor the oxidation of hemes III and IV, it was necessary to assign heme protons in the fully oxidized PpcA (data not shown) using the procedure described by Turner et al. (*35*) for multiheme cytochromes. With the assignment of each heme methyl group in the fully oxidized protein (oxidation stage 3) it was possible to trace back the heme methyl signals from the fully oxidized sample to stage 1 in partially oxidized samples of PpcA, in which stages 3, 2, and 1 coexist.

The paramagnetic chemical shifts of heme methyls $12CH_3^I$, $7^1CH_3^{III}$, and $12^1CH_3^{IV}$ were used to calculate the oxidation fraction of each heme at different stages of oxidation at pH 6.0 and 8.2 (Table 2). Due to the large line widths of the NMR signals in stage 1, it was not possible to observe cross-peaks for heme IV at pH 6.0 and heme III at pH 8.2 (Table 2). Nonetheless, by the fact that the sum of the heme

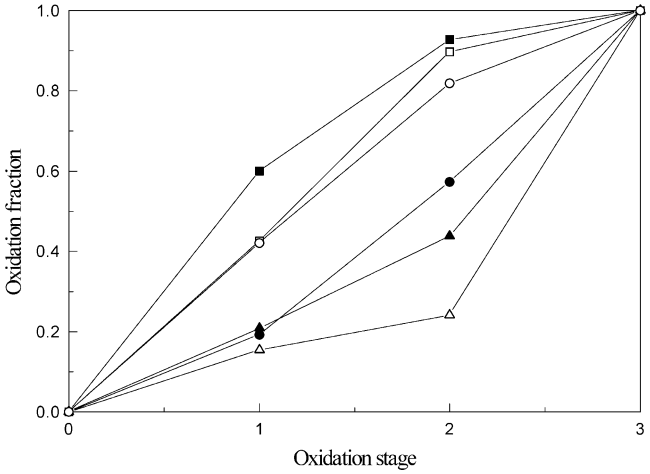

FIGURE 5: Oxidation fraction of the PpcA heme groups in the four oxidation stages at pH 6.0 (solid line and solid symbols) and 8.2 (dashed line and open symbols). Hemes I, III, and IV are represented by squares, triangles, and circles, respectively.

oxidation fractions in oxidation stage 2 is close to 2 (Table 2), it proves that the influence of the oxidation of neighboring hemes on the paramagnetic shift of the heme methyl groups $12^1CH_3^I$, $7^1CH_3^{III}$, and $12^1CH_3^{IV}$ (extrinsic shifts) is not significant. Consequently, in oxidation stage 1 the sum of the heme oxidation fractions is close to 1, allowing for the estimation of heme III and heme IV oxidation fractions at pH 8.2 and pH 6.0, respectively (Table 2).

From the analysis of the heme oxidation fractions obtained at pH 6.0, it is clear that heme I is the heme that becomes more oxidized in the first oxidation step; the largest fractional oxidation of heme IV is obtained in the second step, followed by heme III. Thus, it follows that the order of heme oxidation in PpcA differs from that observed in *Dac*$_7$, in which heme I and III are the first to oxidize to a similar extent, followed by heme IV (*19*). This analysis was performed with a PpcA sample at 500 mM ionic strength, since, as stated before, this is the minimum value for which it is possible to observe the heme NMR signals in all oxidation stages. Previous studies carried out on a related *Desulfovibrio vulgaris* (Miyazaki) cytochrome c_3 showed that microscopic reduction potentials might depend on the ionic strength (*36*). However, from the analysis of the EXSY NMR data obtained for PpcA samples with lower ionic strength than 500 mM (data not shown), it was possible to observe that the order by which the hemes become oxidized does not change.

Redox−Bohr Effect in PpcA. Previous work carried out for the homologue cytochrome *Dac*$_7$ showed that there is no significant redox−Bohr effect in the physiological pH range (*19*). To evaluate the existence of the redox−Bohr effect in PpcA, the order of heme oxidation was also determined at pH 8.2 (Table 2). Contrarily to the case of *Dac*$_7$, in PpcA the results obtained at pH 8.2 showed a dramatic change in the oxidation fractions of the hemes when compared with those obtained at pH 6.0 (Table 2 and Figure 5). In oxidation stage 1 at pH 8.2, the oxidized fractions of hemes I and IV are respectively 42.6% and 42.1% compared with 60% and 19.2%, respectively, measured at pH 6.0. Thus, in comparison with the case of pH 6.0, the oxidized fraction of heme I decreases, and that of heme IV increases. On the other hand, the oxidized fraction of heme III is much less affected by the pH, being 15.3% and 20.8%, at pH 8.2 and 6.0, respectively. Hence, an increase of approximately 2 pH units leads to the increase of the microscopic reduction potential of heme I relative to that of heme IV in such a way that both hemes are oxidized nearly to the same extent in oxidation step 1. At pH 8.2, in the second step of oxidation, heme I is further oxidize by 47.1% and heme IV by 39.8%, so that at oxidation stage 2 they are 89.7% and 81.9% oxidized, respectively. In oxidation stage 2, heme III is only 24.1% oxidized at pH 8.2, whereas at pH 6.0 it was 43.8%. From these results, it is clear that as the oxidized fraction of heme IV in oxidation stage 1 increases (it is more than two times more oxidized at pH 8.2), heme III has a lower tendency to oxidize, reflecting an increase in its reduction potential relative to that of the other hemes. This is clearly illustrated in Figure 5 by comparing the oxidation fraction profiles of the three heme groups at pH 6.0 and 8.2. The changes observed in the redox oxidation profile of the hemes upon pH increase are due to the deprotonation of an ionizable center that modulates the reduction potentials of the individual hemes (redox−Bohr interaction). As a result of the existence of redox−Bohr interactions, heme III dominates even more firmly the oxidation of the protein in the final oxidation step, indicating that, at this pH, its reduction potential is even more separated from those of hemes I and IV.

The analysis of the pH influence on the chemical shifts of the heme methyls $12CH_3^I$, $7^1CH_3^{III}$, and $12^1CH_3^{IV}$ (Table 2) and all the remaining heme methyls (data not shown) in the fully oxidized protein showed that $12^1CH_3^{IV}$ is the most sensitive. The large pH dependence of $12^1CH_3^{IV}$ (2.27 ppm) suggests that the ionizable center responsible for the regulation of the reduction potentials of PpcA heme groups is located close to this heme methyl, which corroborates the large pH dependence of the oxidized fraction of heme IV (Table 2 and Figure 5). From the analysis of PpcA crystal structure, the best candidate to be responsible for the redox−Bohr effect is the carboxylate group of heme IV propionate 13 (IUPAC−IUB nomenclature). To monitor the effect of the protonation of this carboxylate group, heteronuclear multiple quantum coherence NMR experiments were carried out at pH 6.0 and 8.2 (data not shown). Nonetheless, this could not be confirmed, since the NMR signals of the heme IV propionate cannot be confidently assigned at any pH due to the broadness and overlap of the heme propionate signals.

In conclusion, the heme oxidation profiles in PpcA are extremely sensitive to the pH, indicating that the behavior of the redox centers is finely tuned by the pH of the bacterium periplasm. This may prove to be important to ensure an efficient electron transfer to metal ion species.

Redox Titrations Followed by Visible Spectroscopy of PpcA and Its F15 Mutants. The redox titrations of PpcA show that the curve obtained at pH 6.9 is clearly shifted to less negative reduction potential values, when compared to the one obtained at pH 7.9 (Figure 6A). This can be monitored by the apparent midpoint reduction potential, E_{app} (i.e., the point at which the oxidized and reduced fractions of the protein are equal), which increases by 19 mV, and by the macroscopic reduction potentials, which are less negative at pH 6.9 (Table 3). The pH dependence of the redox titration curves in the physiological range (redox−Bohr effect) was also observed for tetraheme cytochromes c_3 (*25*, *29*, *32*, *37*) but not in the PpcA homologue *Dac*$_7$ (*19*). The redox−Bohr

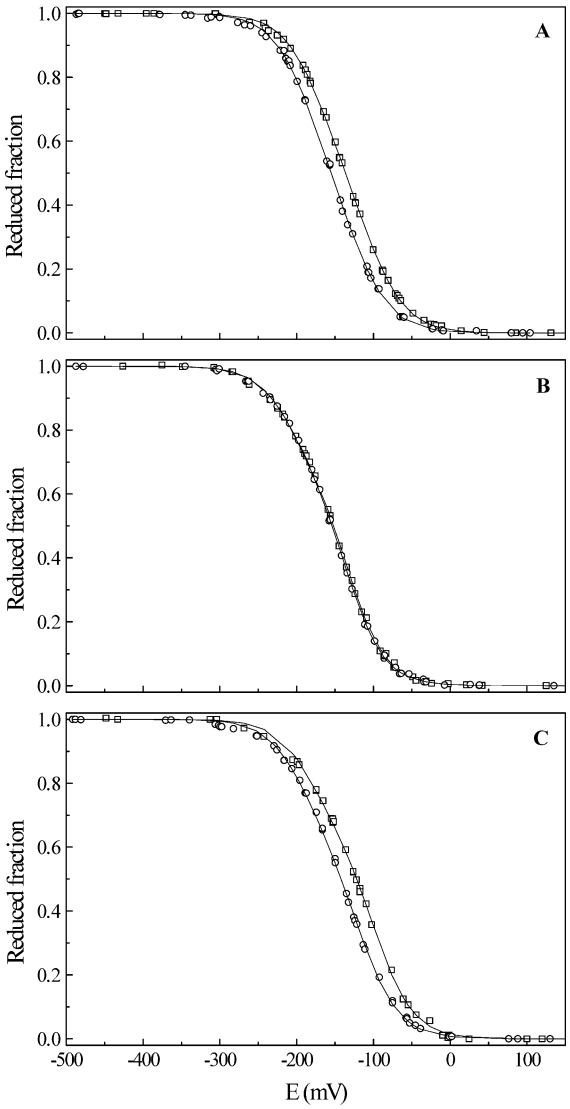

FIGURE 6: Redox titrations followed by visible spectroscopy for PpcA (A), PpcAF15W (B), and PpcAF15Y (C) at pH 6.9 (□) and 7.9 (○). The molar fraction of the total reduced protein was fitted to the model described in MATERIALS AND METHODS. Solid lines indicate the results of the fits for the three macroscopic reduction potentials.

effect allows both a fine regulation of the reduction potential and the coupling between electronic and protonic energy, a key process in bioenergetics (*38*, *39*).

As mentioned before, hemes I and III and F15 form a conserved structural motif that is present in several multiheme cytochromes. This is the case of *D. vulgaris* tetraheme cytochrome c_3, in which F20 is located in an identical spatial position between hemes I and III, as F15 is in PpcA. Biochemical studies were carried out in F20 mutated *D. vulgaris* (Hildenborough) cytochrome c_3 by Saraiva et al. (*40*) and Dolla et al. (*41*).

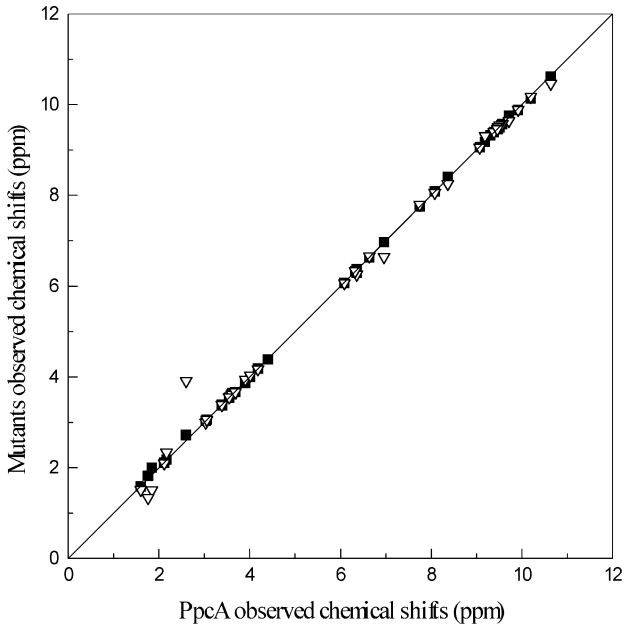

FIGURE 7: Comparison between the chemical shifts observed for heme and F41 aromatic protons of reduced PpcAF15Y (filled squares) and PpcAF15W (open down triangles) and those of PpcA. The dashed line in the figure has a unit slope.

In the present work, to probe a putative functional importance of the conserved phenylalanine residue F15 in PpcA, two different single mutated cytochromes were produced by replacing F15 by tryptophan and tyrosine. The NOESY spectra of PpcAF15Y (Figure 3B) and PpcAF15W (data not shown) are very similar to those of the wild-type (Figure 3A), showing that the general folding and heme core architecture are not affected by the mutations. This is clearly illustrated by the excellent correlation observed between the chemical shifts of the heme protons and the F41 aromatic protons of the mutated cytochromes and those of PpcA (Figure 7). The only signal that is significantly affected in relation to the wild-type protein is heme methyl $12CH_3^1$ in PpcAF15W, reflecting a local structural modification introduced by the larger volume of the tryptophan side chain.

The redox titration of the mutated cytochromes reveals significant modifications of the redox behavior when compared with that of the wild-type protein (Figure 6). The replacement of F15 by tryptophan has a strong effect on the global redox behavior of the protein. Indeed, in PpcAF15W

Table 3: Macroscopic Reduction Potentials and Apparent Midpoint Reduction Potentials for PpcA, PpcAF15W, and PpcAF15Y at pH 6.9 and 7.9[a]

	E_{app} (mV)		E_1 (mV)		E_2 (mV)		E_3 (mV)	
	pH 6.9	pH 7.9	pH 6.9	pH 7.9	pH 6.9	pH 7.9	pH 6.9	pH 7.9
PpcA	−136	−155[b]	−184	−200	−136	−155	−90	−110
PpcAF15W	−152	−154	−209	−209	−146	−148	−115	−117
PpcAF15Y	−122	−142	−184	−198	−116	−138	−80	−99
Dac_7[c]	−168	−168	−219	−218	−169	−169	−112	−112

[a] The macroscopic reduction potentials are the result of the fitting of the reduced fraction of PpcA, PpcAF15W, and PpcAF15Y at each pH value. The apparent midpoint reduction potentials (E_{app}) correspond to the point at which the oxidized and reduced fractions are equal. The reduction potential values are relative to the standard hydrogen electrode. [b] Reference *24*. [c] Values calculated from the experimental data published by Correia et al. (*19*).

the redox−Bohr effect is no longer observed in the physiological pH range, as illustrated by the similarity of all three macroscopic reduction potentials at pH 6.9 and 7.9 (cf. Figure 6A and B; Table 3). Although nonpolar, the presence of an extra NH group in the side chain and also the larger volume of the tryptophan residue (228 Å^3), when compared with the phenylalanine volume (190 Å^3), can easily introduce local structural modifications affecting the degree of protonation of the protein and the concomitant control of the protein redox behavior.

On the other hand, the replacement of F15 by a tyrosine also has a strong effect on the global redox behavior of the protein. Surprisingly, given the more hydrophilic character of tyrosine, this mutation leads to a general increase of the macroscopic reduction potentials (cf. Figure 6A and C, Table 3), shifting to a similar extent the redox curves at both pH values. Although both residues have a similar volume (190 and 194 Å^3, respectively, for phenylalanine and tyrosine), the above observation coupled with NMR results, which show that only minimal structural rearrangements occur in PpcAF15Y (Figure 7), suggests that other factors dominate the changes in the redox behavior of this mutated protein.

The different redox behavior observed upon replacement of the conserved residue F15 in PpcA may result from several simultaneous effects: (i) different H-bond capability of the new amino acid residues when compared with F15; (ii) different solvent accessibility for heme propionates; and (iii) local conformational changes. Altogether, the data obtained for the mutated proteins suggest that F15 plays an important role in the modulation of the PpcA redox behavior. The replacement of a single residue, F15, changes the global redox network tuned to control thermodynamically the electron transfer and may affect the functionality of the protein.

CONCLUSIONS

Specific assignments of NMR resonances to individual heme protons of PpcA allowed the qualitative comparison of the spatial arrangement of the heme core in solution and in the crystal. From the analysis of the interheme NOEs cross-peaks between heme protons and aromatic residues, it was concluded that both the relative position of the three hemes and the general folding of the polypeptide chain are similar in solution and in the crystal.

The results obtained showed that despite the structural similarities observed between PpcA and *Dac*$_7$ these two proteins have different redox properties: the order by which the hemes become oxidized is different (I, IV, III in PpcA and I−III, IV in *Dac*$_7$); the heme oxidation fractions and the macroscopic reduction potentials in PpcA are pH dependent (redox−Bohr effect), whereas in *Dac*$_7$ they are essentially pH independent, in the physiological pH range. The differences observed in the redox properties of PpcA and *Dac*$_7$ may be attributed to different residues surrounding the hemes, as a result of the different primary structures and/or changes in the heme−heme iron distances. The different redox behaviors of those two cytochromes may account for the different functional properties of these proteins, being an excellent example of how structurally related proteins can display functional plasticity leading to different physiological functions.

The results obtained with the mutated proteins PpcAF15W and PpcAF15Y show that the conserved residue F15 has an important function in the control of the redox equilibrium in PpcA, by modulating the reduction potentials, and thus has an important physiological role in this protein.

ACKNOWLEDGMENT

The authors are very grateful to Dr. Ricardo O. Louro for helpful discussions and for critical reading of the manuscript.

SUPPORTING INFORMATION AVAILABLE

Total correlation spectroscopy NMR spectra for PpcA and PpcAF15Y in the reduced form, exchange spectroscopy NMR spectra for PpcA at pH 8.2 illustrating the cross-peaks between heme signals in several different oxidation stages, and a plot with the α-band region of the visible spectra used for the PpcA potentiometric titration carried out at pH 6.9. This material is available free of charge via the Internet at http://pubs.acs.org.

REFERENCES

1. Methé, B. A., Nelson, K. E., Eisen, J. A., Paulsen, I. T., Nelson, W., Heidelberg, J. F., Wu, D., Wu, M., Ward, N., Beanan, M. J., Dodson, R. J., Madupu, R., Brinkac, L. M., Daugherty, S. C., DeBoy, R. T., Durkin, A. S., Gwinn, M., Kolonay, J. F., Sullivan, S. A., Haft, D. H., Selengut, J., Davidsen, T. M., Zafar, N., White, O., Tran, B., Romero, C., Forberger, H. A., Weidman, J., Khouri, H., Feldblyum, T. V., Utterback, T. R., Van Aken, S. E., Lovley, D. R., and Fraser, C. M. (2003) Genome of *Geobacter sulfurreducens*: metal reduction in subsurface environments, *Science 302*, 1967−1969.
2. Lovley, D. R. (2000) Fe(III) and Mn(IV) reduction, in *Environmental microbe-metal interactions* (Lovley, D. R., Ed.) pp 3−30, ASM Press, Washington, DC.
3. Lovley, D. R. (2001) Reduction of iron and humics in subsurface environments, in *Subsurface microbiology and biogeochemistry* (Fredrickson, J. K. F., and Fletcher, M., Ed.) pp 193−217, Wiley-Liss, Inc., New York.
4. Lovley, D. R., and Coates, J. D. (2000) Novel forms of anaerobic respiration of environmental relevance, *Curr. Opin. Microbiol. 3*, 252−256.
5. Lovley, D. R., Baedecker, M. J., Lonergan, D. J., Cozzarelli, I. M., Phillips, E. J., and Siegel, D. I. (1989) Oxidation of aromatic contaminants coupled to microbial reduction, *Nature 339*, 297−299.
6. Rooney-Varga, J. N., Anderson, R. T., Fraga, J. L., Ringelberg, D., and Lovley, D. R. (1999) Microbial communities associated with anaerobic benzene degradation in a petroleum-contaminated aquifer, *Appl. Environ. Microbiol. 65*, 3056−3063.
7. Snoeyenbos-West, O. L., Nevin, K. P., Anderson, R. T., and Lovley, D. R. (2000) Enrichment of *Geobacter* Species in Response to Stimulation of Fe(III) Reduction in Sandy Aquifer Sediments, *Microb. Ecol. 39*, 153−167.
8. Gaspard, S., Vazquez, F., and Holliger, C. (1998) Localization and solubilization of the Iron(III) reductase of *Geobacter sulfurreducens*, *Appl. Environ. Microbiol. 64*, 3188−3194.
9. Leang, C., Coppi, M. V., and Lovley, D. R. (2003) OmcB, a *c*-type polyheme cytochrome, involved in Fe(III) reduction in *Geobacter sulfurreducens*, *J. Bacteriol. 185*, 2096−2103.
10. Lloyd, J. R., Blunt-Harris, E. L., and Lovley, D. R. (1999) The periplasmic 9.6-kilodalton *c*-type cytochrome of *Geobacter sulfurreducens* is not an electron shuttle to Fe(III), *J. Bacteriol. 181*, 7647−7649.
11. Lloyd, J. R., Leang, C., Hodges Myerson, A. L., Coppi, M. V., Cuifo, S., Methe, M., Sandler, S. J., and Lovley, D. R. (2003) Biochemical and genetic characterization of PpcA, a periplasmic *c*-type cytochrome in *Geobacter sulfurreducens*, *Biochem. J. 369*, 153−161.
12. Magnuson, T. S., Isoyama, N., Hodges-Myerson, A. L., Davidson, G., Maroney, M. J., Geesey, G. G., and Lovley, D. R. (2001) Isolation, characterization and gene sequence analysis of a

membrane-associated 89 kDa Fe(III) reducing cytochrome *c* from *Geobacter sulfurreducens*, *Biochem. J. 359*, 147−52.
13. Seeliger, S., Cord-Ruwisch, R., and Schink, B. (1998) A periplasmic and extracellular *c*-type cytochrome of *Geobacter sulfurreducens* acts as a ferric iron reductase and as an electron carrier to other acceptors or to partner bacteria, *J. Bacteriol. 180*, 3686−3691.
14. Afkar, E., and Fukumori, Y. (1999) Purification and characterization of triheme cytochrome c_7 from the metal-reducing bacterium, *Geobacter metallireducens*, *FEMS Microbiol. Lett. 175*, 205−210.
15. Londer, Y. Y., Pokkuluri, P. R., Tiede, D. M., and Schiffer, M. (2002) Production and preliminary characterization of a recombinant triheme cytochrome c_7 from *Geobacter sulfurreducens* in *Escherichia coli*, *Biochim. Biophys. Acta 1554*, 202−211.
16. Pokkuluri, P. R., Londer, Y. Y., Duke, N. E. C., Long, W. C., and Schiffer, M. (2004). Family of cytochrome c_7-type proteins from *Geobacter sulfurreducens*: structure of one cytochrome c_7 at 1.45 Å resolution, *Biochemistry 43*, 849−859.
17. Coutinho, I. B., Turner, D. L., Ming, Y. L., LeGall, J., and Xavier, A. V. (1996) Structure of the three-haem core of cytochrome $c_{551.5}$ determined by ^{1}H NMR, *J. Biol. Inorg. Chem. 1*, 305−311.
18. Turner, D. L., Costa, H. S., Coutinho, I. B., LeGall, J., and Xavier, A. V. (1997) Assignment of the ligand geometry and redox potentials of the trihaem ferricytochrome c_3 from *Desulfuromonas acetoxidans*, *Eur. J. Biochem. 243*, 474−481.
19. Correia, I. J., Paquete, C. M., Louro, R. O., Catarino, T., Turner, D. L., and Xavier, A. V. (2002) Thermodynamic and kinetic characterization of trihaem cytochrome c_3 from *Desulfuromonas acetoxidans*, *Eur. J. Biochem. 269*, 5722−5730.
20. Pfennig, N., and Biebl, H. (1976) *Desulfuromonas acetoxidans* gen. nov. and sp. nov., a new anaerobic, sulfur-reducing, acetate-oxidizing bacterium, *Arch. Microbiol. 110*, 3−12.
21. Brugna, M., Nitschke, W., Toci, R., Bruschi, M., and Giudici-Orticoni, M. T. (1999) First evidence for the presence of a hydrogenase in the sulfur-reducing bacterium *Desulfuromonas acetoxidans*, *J. Bacteriol. 181*, 5505−5508.
22. Czjzek, M., Arnoux, P., Haser, R., and Shepard, W. (2001) Structure of cytochrome c_7 from *Desulfuromonas acetoxidans* at 1.9 Å resolution, *Acta Crystallogr. D57*, 670−678.
23. Aragão, A., Frazão, C., Sieker, L., Sheldrick, G. M., LeGall J., and Carrondo, M. A. (2003) Structure of dimeric cytochrome c_3 from *Desulfovibrio gigas* at 1.2 Å resolution, *Acta Crystallogr. D59*, 644−653.
24. Pokkuluri, P. R., Londer, Y. Y., Norma, E. C., Duke, J. E., Pessanha, M., Salgueiro, C. A., and Schiffer, M. (2004) Structure of a novel c_7-type three-heme cytochrome domain from a multidomain cytochrome *c* polymer, *Protein Sci. 13*, 1684−1692.
25. Louro, R. O., Catarino, T., LeGall, J., Turner, D. L., and Xavier, A. V. (2001) Cooperativity between electrons and protons in a monomeric cytochrome c_3: the importance of mechano-chemical coupling for energy transduction, *ChemBioChem 2*, 831−837.
26. Dutton, P. L. (1978) Redox potentiometry: determination of midpoint potentials of oxidation−reduction components of biological electron-transfer systems, *Methods Enzymol. 54*, 411−435.
27. Gayda, J. P., Benosman, H., Bertrand, P., More, C., and Asso, M. (1988) EPR determination of interaction redox potentials in a multiheme cytochrome: cytochrome c_3 from *Desulfovibrio desulfuricans* Norway, *Eur. J. Biochem. 177*, 199−206.
28. Wang, D. L., Stankovich, M. T., Eng, L. H, and Neujahr, H. Y. (1991) Redox properties of cytochrome c_3 from *Desulfovibrio desulfuricans* NCIMB 8372. Effects of electrode materials and sodium chloride, *J. Electroanal. Chem. 318*, 291−307.
29. Park, J. S., Ohmura, T., Kano, K., Sagara, T., Niki, K., Kyogoku, Y., and Akutsu, H. (1996). Regulation of the redox order of four hemes by pH in cytochrome c_3 from *D. vulgaris* Miyazaki F, *Biochim. Biophys. Acta 1293*, 45−54.
30. Rothery, E. L., Mowat, C. G., Miles, C. S., Walkinshaw, M. D., Reid, G. A., and Chapman, S. K. (2003) Histidine 61: an important heme ligand in the soluble fumarate reductase from *Shewanella frigidimarina*, *Biochemistry 42*, 13160−13169.
31. Pessanha, M., Louro, R. O., Correia, I. J., Rothery, E. L., Pankhurst, K. L., Reid, G. A., Chapman, S. K., Turner, D. L., and Salgueiro, C. A. (2003) Thermodynamic characterization of a tetrahaem cytochrome isolated from a facultative aerobic bacterium, *Shewanella frigidimarina*: a putative redox model for flavocytochrome c_3, *Biochem. J. 370*, 489−495.
32. Turner, D. L., Salgueiro, C. A., Catarino, T., LeGall, J., and Xavier, A. V. (1996) NMR studies of cooperativity in the tetrahaem cytochrome c_3 from *Desulfovibrio vulgaris*, *Eur. J. Biochem. 241*, 723−731.
33. Salgueiro, C. A., Turner, D. L., Santos, H., LeGall, J., and Xavier, A. V. (1992) Assignment of the redox potentials to the four haems in *Desulfovibrio vulgaris* cytochrome c_3 by 2D-NMR, *FEBS Lett. 314*, 155−158.
34. Santos, H., Moura, J. J. G., Moura, I., LeGall, J., and Xavier, A. V. (1984). NMR studies of electron-transfer mechanisms in a protein with interacting redox centres: *Desulfovibrio gigas* cytochrome c_3, *Eur. J. Biochem. 141*, 283−296.
35. Turner, D. L., Salgueiro, C. A., Schenkels, P., LeGall, J., and Xavier, A. V. (1995) Carbon-13 NMR studies of the influence of axial ligand orientation on haem electronic structure, *Biochim. Biophys. Acta 1246*, 24−28.
36. Ohmura, T., Nakamura, H., Niki, K., Cusanovich, M. A., and Akutsu, H. (1998) Ionic strength-dependent physicochemical factors in cytochrome c_3 regulating the electron-transfer rate, *Biophys. J. 3*, 1483−1490.
37. Louro, R. O., Catarino, T., Turner, D. L., Picarra-Pereira, M. A., Pacheco, I., LeGall, J., and Xavier, A. V. (1998) Functional and mechanistic studies of cytochrome c3 from *Desulfovibrio gigas*: thermodynamics of a "proton thruster", *Biochemistry 37*, 15808−15815.
38. Xavier, A. V. (1986) Energy transduction coupling mechanisms in multiredox center proteins, *J. Inorg. Biochem. 28*, 239−243.
39. Xavier, A. V. (2002) A mechano-chemical model for energy transduction in cytochrome *c* oxidase: the work of a Maxwell's god, *FEBS Lett. 532*, 261−266.
40. Saraiva, L. M., Salgueiro, C. A., LeGall, J., van Dougen, W. M. A. M., and Xavier, A. V. (1996) Site-directed mutagenesis of a phenylalanine residue strictly conserved in cytochromes c_3, *J. Biol. Inorg. Chem. 1*, 542−550.
41. Dolla, A., Arnoux, P., Protasevich, I., Lobachov, V., Brugna, M., Giudici-Orticoni, M. T., Haser, R., Czjzek, M., Makarov, A., and Bruschi, M. (1999) Key role of phenylalanine 20 in cytochrome c_3: structure, stability, and function studies, *Biochemistry 38*, 33−41.
42. Piçarra-Pereira, M. A., Turner, D. L., LeGall, J., and Xavier, A. V. (1993). Structural studies on *Desulfovibrio gigas* cytochrome c_3 by two-dimensional ^{1}H-nuclear-magnetic-resonance spectroscopy, *Biochem. J. 294*, 909−915.
43. Messias, A. C., Kastrau, D. H. W., Costa, H. S., LeGall, J., Turner, D. L., Santos, H., and Xavier, A. V. (1998) Solution structure of *Desulfovibrio vulgaris* (Hildenborough) ferrocytochrome c_3: structural basis for functional cooperativity, *J. Mol. Biol. 281*, 719−739.
44. Turner, D. L., Salgueiro, C. A., LeGall, J., and Xavier, A. V. (1992) Structural studies of *Desulfovibrio vulgaris* ferrocytochrome c_3 by two-dimensional NMR, *Eur. J. Biochem. 210*, 931−936.
45. Moss, G. P. (1988) IUPAC−IUB Joint Comission on Biochemical Nomenclature (JCBN), *Eur. J. Biochem. 178*, 277−328.

BI0492859